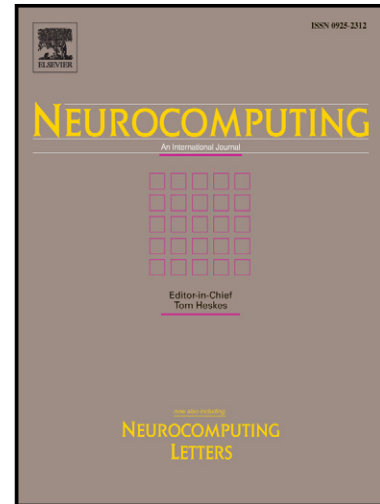


Author's Accepted Manuscript

Fully automatic segmentation of ultrasound common carotid artery images based on machine learning

Rosa-María Menchón-Lara, José Luis Sancho-Gómez



www.elsevier.com/locate/neucom

PII: S0925-2312(14)01303-4
DOI: <http://dx.doi.org/10.1016/j.neucom.2014.09.066>
Reference: NEUCOM14747

To appear in: *Neurocomputing*

Received date: 12 May 2014
Accepted date: 23 September 2014

Cite this article as: Rosa-María Menchón-Lara, José Luis Sancho-Gómez, Fully automatic segmentation of ultrasound common carotid artery images based on machine learning, *Neurocomputing*, <http://dx.doi.org/10.1016/j.neucom.2014.09.066>

This is a PDF file of an unedited manuscript that has been accepted for publication. As a service to our customers we are providing this early version of the manuscript. The manuscript will undergo copyediting, typesetting, and review of the resulting galley proof before it is published in its final citable form. Please note that during the production process errors may be discovered which could affect the content, and all legal disclaimers that apply to the journal pertain.

Fully Automatic Segmentation of Ultrasound Common Carotid Artery Images based on Machine Learning

Rosa-María Menchón-Lara, José Luis Sancho-Gómez

*Dpto. Tecnologías de la Información y las Comunicaciones.
Universidad Politécnica de Cartagena.
Plaza del Hospital, 1, 30202, Cartagena (Murcia), SPAIN.*

Abstract

Atherosclerosis is responsible for a large proportion of cardiovascular diseases (CVD), which are the leading cause of death in the world. The atherosclerotic process is a complex degenerative condition mainly affecting the medium- and large-size arteries, which begins in childhood and may remain unnoticed during decades. It causes thickening and the reduction of elasticity in the blood vessels. An early diagnosis of this condition is crucial to prevent patients from suffering more serious pathologies (heart attacks and strokes). The evaluation of the Intima-Media Thickness (IMT) of the Common Carotid Artery (CCA) in B-mode ultrasound images is considered the most useful tool for the investigation of preclinical atherosclerosis. Usually, it is manually measured by the radiologists. This paper proposes a fully automatic segmentation technique based on Machine Learning and Statistical Pattern Recognition to measure IMT from ultrasound CCA images. The pixels are classified by means of artificial neural networks to identify the IMT boundaries. Moreover, the concepts of Auto-Encoders (AE) and Deep Learning have been included in the classification strategy. The suggested approach is tested on a set of 55 longitudinal ultrasound images of the CCA by comparing the automatic segmentation with four manual tracings.

Keywords: Pattern Recognition, Auto-Encoders, Deep Learning, Atherosclerosis, Ultrasound Imaging, Intima-Media Thickness

Email address: rmml@alu.upct.es (Rosa-María Menchón-Lara)

1. Introduction

Cardiovascular diseases (CVD) represent the major cause of death and disability worldwide. Atherosclerosis is responsible for a large proportion of CVD [1]. It is a chronic degenerative disease characterized by the accumulation of fatty material and cholesterol at the arterial walls. Therefore, atherosclerosis causes thickening and the reduction of elasticity in the arterial walls. Although this pathology may remain unnoticed for decades, atherosclerotic lesions (plaques) could even lead to a total occlusion of the blood vessels. This is the major underlying cause of heart attacks and strokes. For this reason, an early diagnosis and follow up of the atherosclerosis is crucial for preventive purposes. In this sense, the Intima-Media Thickness (IMT) of the Common Carotid Artery (CCA) is considered as an early and reliable indicator of this condition [2].

The IMT is measured by means of a B-mode ultrasound scan, which is a non-invasive, relatively inexpensive, and widely available technique that allows a short time examination. However, resolution and contrast of ultrasound images are generally poor. These images are affected by the multiplicative speckle noise, which tends to reduce the image quality, obscuring and blurring diagnostically important details. The use of different protocols and the variability between observers are recurrent problems in the IMT measurement procedure. Repeatability and reproducibility of the process are of great significance to study the IMT [3, 4]. For these reasons, IMT should be measured preferably on the far wall of the CCA within a region free of plaque [2]. The optimal measurement section (1-cm-long) is located at least 5 mm below the carotid bifurcation, where a double-line pattern corresponding to the intima-media-adventitia layers can be clearly observed. As can be seen in Fig. 1, the IMT is the distance between the lumen-intima (LI) interface and the media-adventitia (MA) interface.

Usually, delineations of the CCA are manually performed by medical experts. By means of image segmentation algorithms it is possible to reduce the subjectivity and variability of manual approaches and detect the IMT throughout the artery length. In the last two decades, several solutions have been developed to perform the carotid wall segmentation in ultrasound images [5]. Most of the proposed methods are not completely automatic and they require user interaction to start the algorithm, such as [6, 7, 8, 9, 10]. However, some fully automatic approaches were recently published [11, 12, 13, 14, 15]. It is possible to make a classification of techniques according to the used methodology. In this sense, we can find algorithms based on edge detection and gradient-based techniques [6, 8, 9, 16], and other proposals based on dynamic programming [17, 18, 19, 20, 21, 22], active

38 contours [7, 12, 23, 24, 25, 26, 27, 28], neural networks [11] or in a combination
 39 of techniques [10, 29, 14]. There are also highlight techniques based in statistical
 40 modeling [30, 31] or in Hough transform [13, 32].

41 In this work, a fully automatic segmentation technique based on Machine
 42 Learning and Statistical Pattern Recognition is proposed to measure IMT from
 43 ultrasound CCA images. Firstly, a given image is pre-processed to detect the re-
 44 gion of interest (ROI). Then, pixels belonging to the ROI are classified by means
 45 of artificial neural networks to identify the LI and MA interfaces. The concepts of
 46 Auto-Encoders (AE) and Deep Learning have been included in this classification
 47 stage. Finally, the obtained results are post-processed to extract the final con-
 48 tours for the IMT measurement. The automatic measures of the IMT have been
 49 compared with the values obtained from different manual segmentations and the
 50 statistical analysis of this comparison shows the accuracy of the proposed method.

51 The remainder of this paper is structured as follows: Sect. 2.1 describes the
 52 dataset of ultrasound CCA images and the manual segmentations. In Sect. 2.2,
 53 the proposed segmentation method is explained in detail. The obtained results are
 54 shown in Sect. 3. Finally, the main extracted conclusions close the paper.

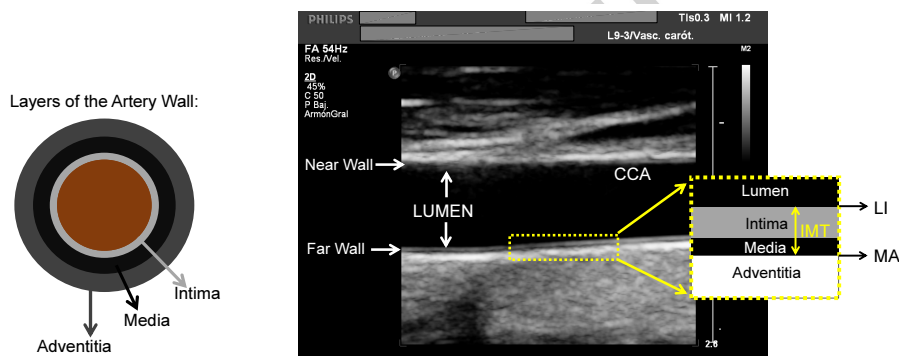


Figure 1: Diagram of the artery wall (left) and longitudinal view of the CCA in a B-mode ultrasound image (right)

55 2. Materials and Methods

56 2.1. Ultrasound Image Acquisition and Manual Segmentations

57 A set of 55 longitudinal B-mode ultrasound images of the CCA have been used
 58 in this work. All of them were provided by the Radiology Department of *Hospi-
 59 tal Universitario Virgen de la Arrixaca* (Murcia, Spain). Fig. 1 (right) shows an

60 example of the tested ultrasound images. Ultrasound scans were acquired using a
 61 *Philips iU22 Ultrasound System* by means of three different ultrasound transduc-
 62 ers (*L12-5*, *L9-3* and *L17-5*) and recorded digitally with 256 gray levels. The spa-
 63 tial resolution of the images ranges from 0.033 to 0.066 mm/pixel, with mean and
 64 standard deviation equal to 0.051 and 0.015 mm/pixel, respectively. The param-
 65 eters of the scanner were adjusted in each case by the radiologist. Some blurred
 66 and noisy images, affected by intraluminal artifacts, and some others with partially
 67 visible boundaries are included in the studied set.

68 To assess the performance of the proposed segmentation method and the accu-
 69 racy of the obtained IMT measurements, it is necessary to compare the automatic
 70 results with some indication of reference values (*ground-truth*, GT). In this case,
 71 the GT corresponds with the average of four different manual segmentations for
 72 each ultrasound image. In particular, two experienced radiologists delineated the
 73 55 images twice, with a mean period of two months between tracings. Each man-
 74 ual segmentation of a given ultrasound image includes tracings for the LI and MA
 75 interfaces on the far carotid wall.

76 2.2. Carotid Ultrasounds Segmentation

77 Fig. 2 shows an overview of the proposed IMT segmentation methodology.
 78 Firstly, a given ultrasound CCA image is pre-processed to automatically detect
 79 the region of interest (ROI), which is the far wall of the blood vessel. As result
 80 of this stage, a cropping of the input ultrasound image is obtained (ROI image).
 81 Then, a windowing process takes place on the ROI image in order to construct the
 82 intensity pattern corresponding to each pixel (intensity values from a neighbour-
 83 hood). After this, different auto-encoders provide compressed representations of
 84 these intensity patterns in a lower dimensional feature space. The new features
 85 are classified by means of artificial neural networks to separately detect the LI
 86 and MA interfaces. Finally, classification results are post-processed to extract the
 87 final contours on which the IMT is measured.

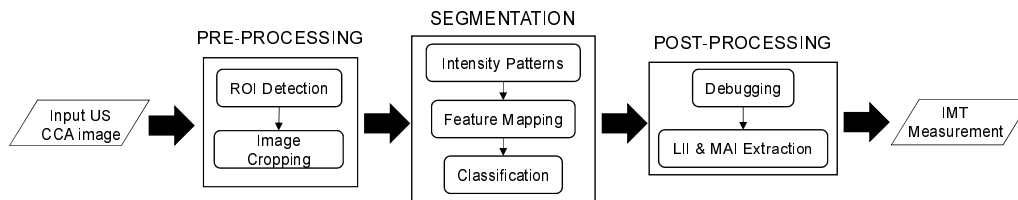


Figure 2: Overview of the proposed method for carotid wall segmentation and IMT measurement

88 2.2.1. Pre-processing of ultrasound CCA images

89 In the carotid ultrasound images (see Fig. 1), the lumen corresponds to a dark
90 region (low echogenicity) delimited by the arterial walls. Over the lumen in the
91 picture, at less depth, it is observed the echo corresponding to the near wall. The
92 far wall, where the IMT is measured, is located below the lumen, and it constitutes
93 the region of interest (ROI).

94 The aim of the pre-processing stage is the location of the carotid far wall in a
95 completely automatic way. In particular, a binary mask is built using morphologi-
96 cal operations [33] to locate the carotid lumen. Once the lumen has been located,
97 we focus on its lower limit corresponding to the far wall of the CCA and the
98 boundaries of the ROI are established. The superior boundary is fixed to 0.6 mm
99 above the upper point of the far wall detected in the binary mask, whereas the bot-
100 tom boundary is fixed to 1.5 mm below the lower point. As result of this stage, a
101 cropping of the input ultrasound image is obtained (ROI image). For more details
102 about this stage consult [11].

103 2.2.2. Segmentation by means of Pattern Recognition with Neural Networks

104 Segmentation is one of the most difficult tasks in nontrivial image process-
105 ing. Since segmentation can be considered as a classification of pixels, it is often
106 treated as a pattern recognition problem and addressed with related techniques
107 [34]. This section describes the main stage of the proposed method, in which ar-
108 tificial Neural Networks (NN) carry out the segmentation of the ultrasound CCA
109 images. The NN used in this work are standard *Multi-Layer Perceptrons* (MLP),
110 with a single hidden layer, trained under the *Scaled Conjugate Gradient* (SCG)
111 learning rule [35].

112 The initial idea consists of training NN to classify the pixels from the ultra-
113 sound images by considering the intensity values of a neighbourhood of the pixel
114 to classify [11]. The neighbourhoods considered in this study are vertically ori-
115 ented rectangular windows (13×3 pixels), since the '*bright-dark-bright*' inten-
116 sity pattern corresponding to the IMT can be found in the vertical direction of the
117 images. The reason for choosing a window height of 13 pixels is that for the used
118 set of 55 ultrasound CCA images, the mean IMT is about 13 pixels. Therefore,
119 this neighbourhood will provide the best contextual information about the pixel
120 to be classified. After the appropriate learning process, a given network will be
121 able to recognize the pixels belonging to the IMT boundaries (i.e., LI and MA
122 interfaces). Furthermore, in this paper, the concepts of Auto-Encoders (AE) and
123 Deep Learning have been incorporated to the original scheme. Fig. 3 shows the
124 proposed configuration. As can be seen in the scheme, the processing of each IMT

125 boundary (LI and MA interfaces) is separately performed.

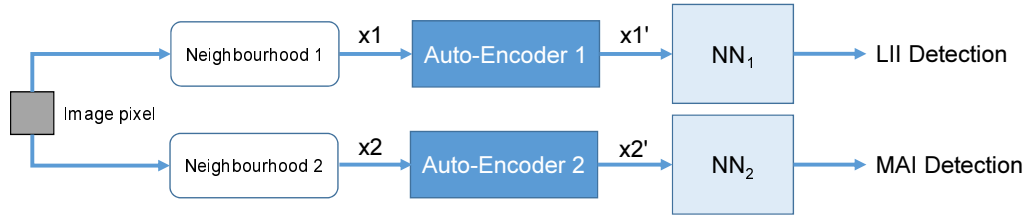


Figure 3: Strategy adopted to solve the segmentation task

126 Auto-Encoders 1 and 2 are artificial NN used for learning efficient codifica-
 127 tions. AE learns to represent features in a dataset meaningfully, typically for the
 128 purpose of dimensionality reduction [36]. It was shown that those are more effi-
 129 cient than other methodologies such as Principal Component Analysis (PCA) [37].
 130 The AE proposed here are MLP performing unsupervised learning, in which input
 131 data is used as output data (see Fig. 4). Then, in the hidden layer of the AE take
 132 place a feature mapping. In our particular case, $M < d$ (number of hidden neurons
 133 $<$ input data dimension, see Fig. 4), and a compressed representation of the data
 134 is obtained at the output of the AE hidden layer. These outputs of the hidden layer
 135 are then used as input data to another MLP (NN_1 or NN_2 in 2) for its classification.

136 A dataset is needed to perform the training of the different NN. To ensure a
 137 good generalization capability of the networks, five heterogeneous images were
 138 carefully chosen (with different orientations of the CCA, spatial resolutions, IMT
 139 measures, etc.) to assemble a representative and consistent dataset. It is necessary
 140 to emphasize that using all the pixels/patterns in a selected image for training is

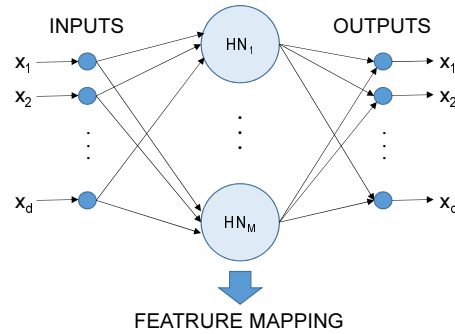


Figure 4: Structure of a generic Auto-Encoder

141 inappropriate, since the dataset would be extremely large and highly imbalanced.
 142 In our case, the dataset was assembled by taking samples from the five manually
 143 segmented images selected for this purpose. Finally, it consists of 12,900 patterns:
 144 3,100 of them (24%) are from class '*LII-pixels*'; 3,350 (26%) are from class '*MAI-*
 145 *pixels*'; and the remaining (50%) are from class '*non-IMT-boundary*'. During
 146 the learning process, the dataset was randomly divided into three subsets: 50%
 147 of samples for training, 20% for validation (stopping criterion and network size
 148 selection) and 30% for testing.

149 As commented above, the LI and MA interfaces are separately detected. For
 150 the LI interface, AE_1 is trained to obtain compressed representations of the pat-
 151 terns corresponding to pixels belonging to the LI interface (3,100 patterns with
 152 a dimension of $13 \times 3 = 39$ features). The learning process is repeated vary-
 153 ing the number of hidden neurons of the AE_1 from 2 to 39. Then, the whole
 154 dataset (12,900 patterns) is passed through the AE_1 and the hidden layer outputs
 155 are used to train NN_1 , which performs a binary classification between '*LII-pixels*'
 156 and '*non-LII-pixels*'. On the other hand, AE_2 performs a feature mapping for pat-
 157 terns corresponding to pixels belonging to the MA interface (3,350 patterns with
 158 39 features). Once its training is carried out, the 12,900 samples are processed
 159 with AE_2 . The transformed features (hidden layer outputs) are used in the learn-
 160 ing process of the NN_2 , which performs another binary classification between
 161 '*MAI-pixels*' and '*non-MAI-pixels*'.

162 Moreover, as it shown in Fig. 3, two neighbourhoods have been considered.
 163 For both AE_1 and AE_2 , the input patterns consist of 39 features (13×3 win-
 164 dow). However, whereas for AE_2 the neighbourhood is centred on the pixel to be
 165 classified, for the AE_1 the neighbourhood is vertically displaced until the pixel to
 166 classify is located at the central position of the window base. This is done with
 167 the purpose of providing a better characterization of the '*LII-pixels*' to AE_1 (large
 168 dark area corresponding to the lumen above the pixel).

169 As it shown in Sect. 3.1, the use of auto-encoders allows a significant reduc-
 170 tion in the dimension of the features space (from 39 to 11 for AE_1 , and from 39 to
 171 9 for AE_2). Fig. 7 (central) shows the final classification results for an ultrasound
 172 CCA image, according to the proposed classification scheme. As can be seen, the
 173 LI and MA interfaces are correctly identified in the image. Nevertheless, it is still
 174 necessary to eliminate some residues and to refine the contours in order to assess
 175 the IMT. To this end, a post-processing stage has been designed (detailed in Sect.
 176 2.2.3).

177 2.2.3. *Post-processing of Classification Results*

178 The results of the classification stage should be debugged to extract the final
179 LI and MA boundaries, see central image in Fig. 7. It is necessary to identify
180 and discard, as far as possible, the mis-classified pixels. In this sense, the
181 relative position between pixels classified as '*LII-pixels*' and those classified as
182 '*MAI-pixels*' provides useful information. Moreover, due to the poor resolution
183 of the ultrasound images, thick boundaries are obtained instead of one-pixel contours.
184 This happens because the networks find the searched intensity patterns in
185 all these pixels. In order to solve this drawback, a simple non-linear data-fitting
186 problem is formulated to find the best polynomial approximation for LI and MA
187 interfaces. This is done by minimizing the squared error between the LII-pixels
188 (or MAI-pixels) in the image and the approximated contour. The bottom image
189 in Fig. 7 (bottom) shows an example of the final boundaries extracted from the
190 classification results (central image).

191 3. Results

192 The suggested segmentation methodology was developed and tested in a PC
193 with a core i7-3770 3.4 GHz processor and 12 GB RAM running MATLAB
194 2013a. The mean total time per processed image is 1.4 s. The ROI selection
195 task (pre-processing stage) shows high computational efficiency by spending 0.37
196 s in mean for each case. Once the networks have been trained, classification results
197 are provided in a fast way, with an average response time of 0.48 s for all the
198 pixel in the selected ROI. On the other hand, the post-processing returns the final
199 IMT boundaries in 0.6 seconds.

200 3.1. *Feature Mapping and Classification Performance*

201 As commented in Sect. 2.2.2, AE_1 and AE_2 are trained to obtain a compressed
202 representation ($M < d$, see Fig. 4) of the intensity pattern corresponding to each
203 pixel of a given ultrasound CCA image. In each case, the learning process is repeated
204 varying the number of hidden neurons from 2 to 39. For each network size
205 (number of hidden nodes), the corresponding NN_1 and NN_2 (with different
206 dimension of input data) were trained and its performance has been analysed. All
207 designed networks in this study were retrained 30 times with different initial random
208 values of the connection weights. Moreover, the number of hidden neurons
209 in NN_1 and NN_2 is varied from 5 to 100 and the optimal size of each network is
210 selected according to the minimum mean error reached on a validation dataset.

211 Fig. 5 shows the performance of NN_1 in each case (from 2 to 39 input fea-
 212 tures). The mean classification accuracy achieved is depicted in the left graph,
 213 whereas the mean specificity and sensitivity are shown in the right graphic. NN_1
 214 together with AE_1 outperform the classification accuracy of a MLP trained with
 215 the 39-dimensional data (13×3 neighbourhood) to recognize the LI interface
 216 (dashed line in Fig. 5) when considering a feature mapping to 3 or more dimen-
 217 sions. Since the specificity remains constant, the optimal configuration has been
 218 chosen by analysing the sensitivity. Thus, the best performance is obtained with
 219 11 input features, i.e. when AE_1 reduces the dimensionality of data from 39 to
 220 11. In a similar way, Fig. 6 shows the performance of NN_2 , which was trained to
 221 identify ‘MAI-pixels’. In this case, AE_2 and NN_2 achieve a classification accuracy
 222 similar to the obtained when considering a 39-dimensional feature space (dashed
 223 line). The optimal configuration (best sensitivity) is obtained for 9 input features
 224 (feature mapping from 39 to 9 dimensions).

225 3.2. Segmentation Accuracy and IMT Measurements

226 The proposed segmentation method has been tested on a set of 55 B-mode.
 227 Some examples of segmented images are shown in Figs. 7 and 8. The final bound-
 228 aries corresponding to the LI and MA interfaces detected by our automatic seg-
 229 mentation method are superimposed on the ultrasounds. As can be seen, our fully
 230 automatic segmentation approach is robust against the orientation and appearance
 231 of the CCA in the ultrasound image (slope and curvature).

232 Given an ultrasound image and two different segmentations (S_1 and S_2) to
 233 compare, the degree of agreement between its IMT measures is assessed by cal-

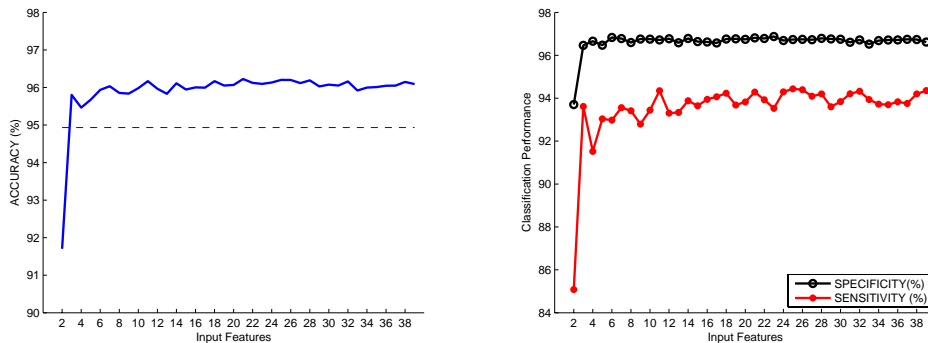


Figure 5: Performance of NN_1 (trained to detect LII-pixels) for different dimensions of input data: mean classification accuracy (left); specificity and sensitivity (right)

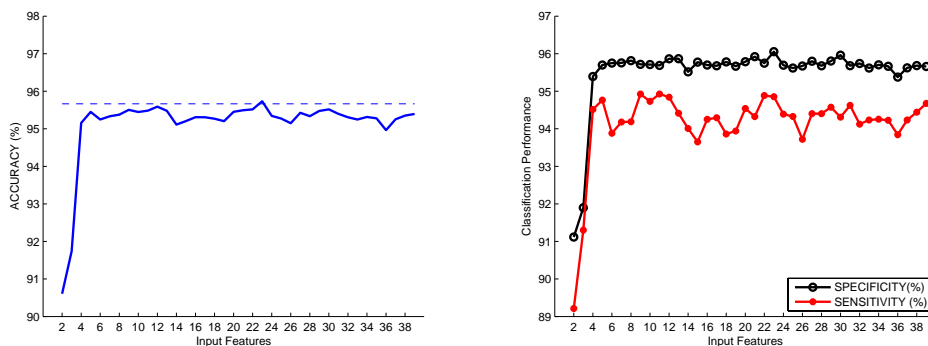


Figure 6: Performance of NN_2 (trained to detect MAI-pixels) for different dimensions of input data: mean classification accuracy (left); specificity and sensitivity (right)

234 culating the absolute error value:

$$\epsilon^{IMT_i} = |IMT_i^{S_1} - IMT_i^{S_2}| \quad (1)$$

235 being ϵ^{IMT_i} the IMT measurement error between the segmentation S_1 and the
 236 segmentation S_2 for the i -th image. In each case, the IMT value, i.e. the dis-
 237 tance between the boundaries corresponding to LI and MA, is evaluated by using
 238 the Mean Absolute Distance (MAD) metric. The mean and standard deviation
 239 values (55 processed images) for the intra-observer (E_{1_1} - E_{1_2} and E_{2_1} - E_{2_2}), inter-
 240 observer (E_1 - E_2) and inter-method (A-GT) IMT measurement errors can be seen
 241 in Table 1. The mean absolute error of the automatic measurements is about 50
 242 μm , which is a value slightly higher than the intra- and inter-observer errors but it
 243 is similar to the obtained by other published methods (see Table 2).

244 Moreover, Fig. 9 shows the linear regression analysis for the IMT mea-
 245 sures between manual and automatic segmentations (right graph), and the Bland-
 246 Altman plots of the differences between the IMT of the corresponding two seg-
 247 mentations (manual and automatic) against their average (left graph). The regres-
 248 sion analysis shows a high degree of agreement between manual and automatic
 249 measurements, with a 93.3 % correlation coefficient. Bland-Altman plot shows
 250 the following limits of agreement (mean $\pm 2 \times$ standard deviation): $-0.018 \pm$
 251 0.137 mm. Therefore, the proposed method tends to slightly underestimate the
 252 IMT.

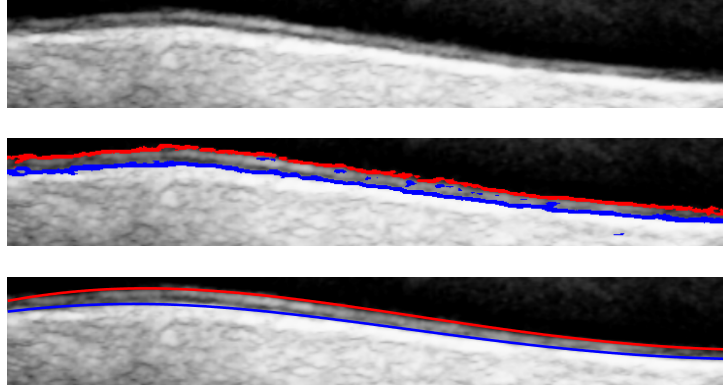


Figure 7: Example of the results obtained at each stage of the proposed segmentation method: selected ROI in the pre-processing stage (top); classification results (central); final LI and MA boundaries after the post-processing stage

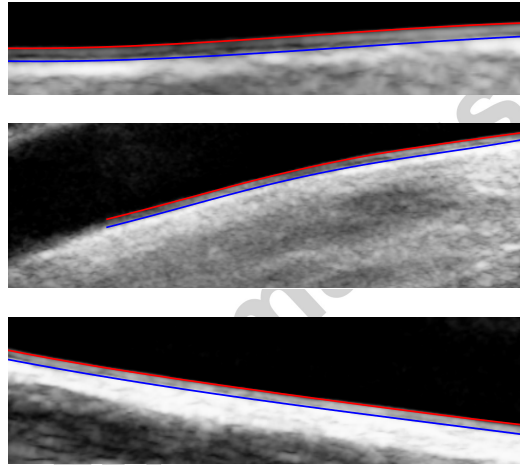


Figure 8: Different examples of good segmentation. The proposed method is robust against the orientation and appearance of the CCA in the ultrasound image

253 4. Conclusions

254 This paper proposes a fully automatic segmentation method of the CCA far
 255 wall based on Machine Learning in order to measure the IMT. Segmentation is
 256 treated as a pattern recognition problem. Thus, the main stage of the proposed
 257 technique is a classification stage, in which different neural networks perform
 258 a classification of the image pixels to detect the IMT contours (LI and MA in-
 259 terfaces). Networks take as input information only the intensity values from a

Table 1: IMT measurement errors (mm) between different segmentations

	IMT Measurement Error	
	Mean	Std. Dev.
$E1_1-E1_2$	0.025	0.018
$E2_1-E2_2$	0.027	0.021
$E1-E2$	0.037	0.069
$A-GT$	0.050	0.050

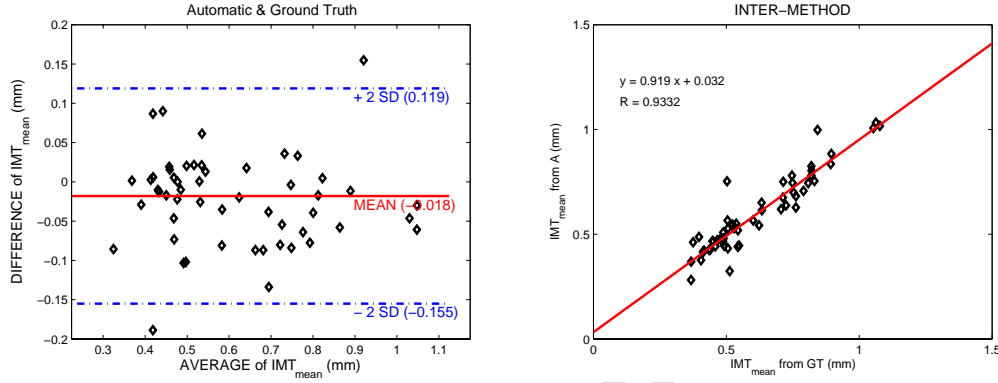


Figure 9: Statistical distribution of the IMT measurement errors. BlandAltman plot (left) and linear regression analysis (right)

260 neighbourhood (13×3) of the pixel to be classified. The suggested architecture
 261 includes auto-encoders to obtain compressed and efficient representations of the
 262 input data. These auto-encoders establish the basis for the design of deep net-
 263 works to identify LII-pixels and MAI-pixels. The system is completed with a
 264 pre-processing stage in which ROI (far wall of the CCA) is automatically selected
 265 and with a post-processing stage for the extraction of the final contours on which
 266 the IMT is assessed.

267 The proposed configuration has been tested using a set of 55 ultrasound CCA
 268 images. The automatic segmentation achieves the correct detection of the LI and
 269 MA interfaces in all the tested images. Furthermore, the automatic measurements
 270 of IMT have been compared with the values obtained from manual tracings and
 271 several quantitative statistical evaluations have shown the accuracy and robustness
 272 of the suggested approach.

273 The main advantage of the CCA segmentation method proposed in this pa-

Table 2: Comparison with other techniques for the IMT measurement. The metric adopted to assess the IMT and the errors is MAD. N is the number of images and the third column shows the spatial resolution of the images in mm/pixel. FA: Fully Automatic

Author	N	IMT _{GT} (mm)	IMT _{Method} (mm)	ϵ^{IMT} (μm)	FA
Liang [18]	50	0.88 \pm 0.25	0.93 \pm 0.25	42 \pm 25	NO
Liguori [6]	20	0.92 \pm 0.19	0.92 \pm 0.20	15.6 \pm 4.2	NO
Gutierrez [24]	30	0.63 \pm 0.12	0.72 \pm 0.14	90 \pm 60	NO
Stein [8]	50	-	0.67 \pm 0.12	40 \pm 7	NO
Faita [9]	150	0.56 \pm 0.14	0.57 \pm 0.14	10 \pm 35	NO
Molinari [14]	182	0.92 \pm 0.30	0.75 \pm 0.39	54 \pm 35	YES
Xu [32]	50	0.63 \pm 0.14	0.65 \pm 0.16	38.1 \pm 16.4	NO
Petroudi [28]	100	0.67 \pm 0.14	0.61 \pm 0.15	95.0 \pm 61.5	NO
Menchón-Lara [11]	60	0.64 \pm 0.19	0.61 \pm 0.19	37.6 \pm 25.2	YES
Proposed Method	55	0.62 \pm 0.19	0.60 \pm 0.19	49.9 \pm 49.8	YES

274 per is its computational efficiency, with a mean total time per processed image of
 275 1.4 seconds. This fact together with the high agreement between automatic and
 276 manual segmentations make this method a suitable solution for the clinical eval-
 277 uation of IMT. Besides, with this average execution time, the method could also
 278 be used for the segmentation of ultrasound CCA videos. Future works must study
 279 the use of different learning machines (support vector machines, extreme learning
 280 machines) to construct the proposed deep networks. However, although the MLP
 281 solution used in this work seems to be the simplest, it provides quite satisfactory
 282 results.

References

- [1] W. H. Organization, Global atlas on cardiovascular disease prevention and control, online.
URL www.who.int/cardiovascular_diseases/en/
- [2] P.-J. Touboul, et al., Mannheim carotid intima-media thickness and plaque consensus (2004-2006-2011), *Cerebrovascular Diseases* 34 (2012) 290–296.
- [3] M. Bots, Evans, G.W., W. Riley, D. Grobbee, Carotid intima-media thickness measurements in intervention studies: design options, progression rates, and sample size considerations: a point of view, *Stroke* 34 (12) (2003) 2985–2994.

- [4] J. Gonzalez, J. Wood, F. J. Dorey, T. A. L. Wren, V. Gilsanz, Reproducibility of carotid intima-media thickness measurements in young adults, *Radiology* 247 (2) (2008) 465–247.
- [5] F. Molinari, G. Zeng, J. S. Suri, Review: A state of the art review on intima-media thickness (imt) measurement and wall segmentation techniques for carotid ultrasound, *Comput. Methods Prog. Biomed.* 100 (3) (2010) 201–221.
- [6] C. Liguori, A. Paolillo, A. Pietrosanto, An automatic measurement system for the evaluation of carotid intima-media thicknesss, *Instrumentation and Measurement, IEEE Transactions on* 50 (6) (2001) 1684–1691.
- [7] D.-C. Cheng, A. Schmidt-Trucksass, K.-S. Cheng, H. Burkhardt, Using snakes to detect the intimal and adventitial layers of the common carotid artery wall in sonographic images, *Computers Methods and Programs in Biomedicine* 67 (1) (2002) 27–37.
- [8] J. H. Stein, C. E. Korcarz, M. E. Mays, P. S. Douglas, M. Palta, H. Zhang, T. LeCaire, D. Paine, D. Gustafson, L. Fan, A semiautomated ultrasound border detection program that facilitates clinical measurement of ultrasound carotid intima-media thickness, *Journal of the American Society of Echocardiography* 18 (3) (2005) 244–251.
- [9] F. Faita, V. Gemignani, E. Bianchini, C. Giannarelli, L. Ghiadoni, M. Demi, Real-time measurement system for evaluation of the carotid intima-media thickness with a robust edge operator, *Journal of ultrasound in medicine* 27 (9) (2008) 1353–1361.
- [10] R. Rocha, A. Campilho, J. Silva, E. Azevedo, R. Santos, Segmentation of the carotid intima-media region in b-mode ultrasound images, *Image and Vision Computing* 28 (4) (2010) 614–625.
- [11] R.-M. Menchón-Lara, M.-C. Bastida-Jumilla, J. Morales-Sánchez, J.-L. Sancho-Gómez, Automatic detection of the intima-media thickness in ultrasound images of the common carotid artery using neural networks, *Medical & Biological Engineering & Computing* 52 (2) (2014) 169–181.
- [12] S. Delsanto, F. Molinari, P. Giusetto, W. Liboni, S. Badalamenti, J. Suri, Characterization of a completely user-independent algorithm for carotid

- artery segmentation in 2-d ultrasound images, *IEEE Transactions on Instrumentation and Measurement* 56 (4) (2007) 1265–1274.
- [13] S. Golemati, J. Stoitsis, E. G. Sifakis, T. Balkizas, K. S. Nikita, Using of the hough transform to segment ultrasound images of longitudinal and transverse sections of the carotid artery, *Ultrasound in Medicine & Biology* 33 (12) (2007) 1918–1932.
- [14] F. Molinari, G. Zeng, J. Suri, Intima-media thickness: setting a standard for a completely automated method of ultrasound measurement, *Ultrasonics, Ferroelectrics and Frequency Control, IEEE Transactions on* 57 (5) (2010) 1112–1124.
- [15] M. C. Bastida-Jumilla, R. M. Menchón-Lara, J. Morales-Sánchez, R. Verdú-Monedero, J. Larrey-Ruiz, J. L. Sancho-Gómez, Segmentation of the common carotid artery walls based on a frequency implementation of active contours, *Journal of Digital Imaging* 26 (1) (2013) 129–139.
- [16] R. H. Selzer, W. J. Mack, P. L. Lee, H. Kwong-Fu, H. N. Hodis, Improved common carotid elasticity and intima-media thickness measurements from computer analysis of sequential ultrasound frames, *Atherosclerosis* 154 (1) (2001) 185 – 193.
- [17] I. Wendelhag, Q. Liang, T. Gustavsson, J. Wikstrand, A new automated computerized analysis system simplifies readings and reduces the variability in ultrasound measurement of intima-media thickness, *Stroke* 28 (1997) 2195–2200.
- [18] Q. Liang, I. Wendelhag, J. Wikstrand, T. Gustavsson, A multiscale dynamic programming procedure for boundary detection in ultrasonic artery images, *Medical Imaging, IEEE Transactions on* 19 (2) (2000) 127–142.
- [19] T. Gustavsson, Q. Liang, I. Wendelhag, J. Wikstrand, A dynamic programming procedure for automated ultrasonic measurement of the carotid artery, in: *Computers in Cardiology 1994*, 1994, pp. 297–300.
- [20] D.-C. Cheng, X. Jiang, Detections of arterial wall in sonographic artery images using dual dynamic programming, *Information Technology in Biomedicine, IEEE Transactions on* 12 (6) (2008) 792 –799.

- [21] N. Santhiyakumari, M. Madheswaran, Non-invasive evaluation of carotid artery wall thickness using improved dynamic programming technique, *Signal, Image and Video Processing* 2 (2) (2008) 183–193.
- [22] Y.-B. Lee, Y.-J. Choi, M.-H. Kim, Boundary detection in carotid ultrasound images using dynamic programming and a directional haar-like filter, *Computers in Biology and Medicine* 40 (8) (2010) 687 – 697.
- [23] R. Chan, J. Kaufhold, L. Hemphill, R. Lees, W. Karl, Anisotropic edge-preserving smoothing in carotid b-mode ultrasound for improved segmentation and intima-media thickness (imt) measurement, in: *Computers in Cardiology 2000*, 2000, pp. 37–40.
- [24] M. Gutierrez, P. Pilon, S. Lage, L. Kopel, R. Carvalho, S. Furuie, Automatic measurement of carotid diameter and wall thickness in ultrasound images, in: *Computers in Cardiology*, 2002, 2002, pp. 359–362.
- [25] C. P. Loizou, C. S. Pattichis, M. Pantziaris, T. Tyllis, A. Nicolaides, Snakes based segmentation of the common carotid artery intima media, *Medical and biological engineering and computing* 45 (1) (2007) 35–49.
- [26] M. Ceccarelli, N. De Luca, A. Morganella, An active contour approach to automatic detection of the intima-media thickness, in: *2006 IEEE International Conference on Acoustics, Speech and Signal Processing. ICASSP 2006 Proceedings.*, Vol. 5, 2006, pp. 709–712.
- [27] F. Molinari, K. M. Meiburger, L. Saba, U. R. Acharya, M. Ledda, A. Nicolaides, J. S. Suri, Constrained snake vs. conventional snake for carotid ultrasound automated imt measurements on multi-center data sets, *Ultrasonics* 52 (7) (2012) 949 – 961.
- [28] S. Petroudi, C. Loizou, M. Pantziaris, C. Pattichis, Segmentation of the common carotid intima-media complex in ultrasound images using active contours, *IEEE Transactions on Biomedical Engineering* 59 (11) (2012) 3060–3069.
- [29] G. Liu, B. Wang, D. Liu, Detection of intima-media layer of common carotid artery with dynamic programming based active contour model, in: *Pattern Recognition, 2008. CCPR '08. Chinese Conference on*, 2008, pp. 1–6.

- [30] F. Destrempe, J. Meunier, M.-F. Giroux, G. Soulez, G. Cloutier, Segmentation in ultrasonic b-mode images of healthy carotid arteries using mixtures of nakagami distributions and stochastic optimization, *Medical Imaging, IEEE Transactions on* 28 (2) (2009) 215–229.
- [31] D. Ilea, P. Whelan, C. Brown, A. Stanton, An automatic 2d cad algorithm for the segmentation of the imt in ultrasound carotid artery images, in: *Engineering in Medicine and Biology Society, 2009. EMBC 2009. Annual International Conference of the IEEE, 2009*, pp. 515–519.
- [32] X. Xu, Y. Zhou, X. Cheng, E. Song, G. Li, Ultrasound intima-media segmentation using hough transform and dual snake model, *Computerized Medical Imaging and Graphics* 36 (3) (2012) 248–258.
- [33] R. C. González, R. E. Woods, S. L. Eddins, *Digital Image Processing using Matlab*, Pentice Hall, 2004.
- [34] D. Pham, C. Xu, J. Prince, Current methods in medical image segmentation, *Annual Review of Biomedical Engineering* 2 (2000) 315–337.
- [35] M. Moller, A scaled conjugate gradient algorithm for fast supervised learning, *Neural Networks* 6 (1993) 525–533.
- [36] G. E. Hinton, R. R. Salakhutdinov, Reducing the dimensionality of data with neural networks, *Science* 313 (5786) (2006) 504–507.
- [37] L. L. C. Kasun, H. Zhou, G.-B. Huang, C. M. Vong, Representational learning with extreme learning machine for big data, *IEEE Intelligent Systems* 28 (6) (2013) 31–34.
- [38] C. M. Bishop, *Pattern Recognition and Machine Learning*, Springer, 2006.